

August 2007

# A device-level vacuum-packaging scheme for microbolometers on rigid and flexible substrates

Aamer Mahmood

*Birck Nanotechnology Center, Purdue University, amahmood@purdue.edu*

Donald P. Butler

*Department of Electrical Engineering, University of Texas at Arlington*

Zeynep Celik-Butler

*Department of Electrical Engineering, University of Texas at Arlington*

Follow this and additional works at: <http://docs.lib.purdue.edu/nanopub>

---

Mahmood, Aamer; Butler, Donald P.; and Celik-Butler, Zeynep, "A device-level vacuum-packaging scheme for microbolometers on rigid and flexible substrates" (2007). *Birck and NCN Publications*. Paper 300.  
<http://docs.lib.purdue.edu/nanopub/300>

This document has been made available through Purdue e-Pubs, a service of the Purdue University Libraries. Please contact [epubs@purdue.edu](mailto:epubs@purdue.edu) for additional information.

# A Device-Level Vacuum-Packaging Scheme for Microbolometers on Rigid and Flexible Substrates

Aamer Mahmood, *Student Member, IEEE*, Donald P. Butler, *Senior Member, IEEE*, and Zeynep Çelik-Butler, *Senior Member, IEEE*

**Abstract**—This paper reports on the design, fabrication, and characterization of device-level vacuum-packaged microbolometers on rigid Si wafers and flexible polyimide substrates. Semiconducting yttrium barium copper oxide (commonly referred to as YBCO) serves as the bolometric material. Operating micromachined bolometers in vacuum reduces the thermal conductance  $G_{th}$  from the detector to the substrate. If flexibility of the substrate is not to be sacrificed, then the vacuum packaging needs to be done at the device level. Here, the microbolometers are fabricated on a silicon nitride support membrane, isolated from the substrate using surface micromachining. Suitable materials as well as various dimensions in the vacuum cavity are determined using finite-element method (FEM)-based CoventorWARE. A vacuum cavity made of  $Al_2O_3$  has been designed. The thermal conductance  $G_{th}$  of bolometers with the geometry implemented in this work is the same for devices on rigid and flexible substrates. The theoretical value of  $G_{th}$  was calculated to be  $4.0 \times 10^{-6}$  W/K for devices operating in vacuum and  $1.4 \times 10^{-4}$  W/K for devices operating at atmospheric pressure. Device-level vacuum-packaged microbolometers on both rigid Si and flexible polyimide substrates have been fabricated and characterized for optical and electrical properties. A low thermal conductance of  $1.1 \times 10^{-6}$  W/K has been measured six months after fabrication, which implies an intact vacuum cavity.

**Index Terms**—Bolometer, flexible substrates, packaging, smart skin.

## I. INTRODUCTION

**F**LEXIBLE electronics has attracted considerable interest in recent years. Advances in integrated electronics and the advent of MEMS promise complete miniature systems, comprising of sensors, electronics, actuators, and power sources within the same chip. Flexible substrate systems and electronics can be made to conform to nonplanar host surfaces. This is useful not only for new systems designed from scratch but also for upgrades to existing platforms. A case in point would be

Manuscript received October, 23, 2006; accepted; December 13, 2006. This work was supported in part by the National Science Foundation under Grant ECS-0401148 and in part by the Semiconductor Research Corporation under Grant 2004-RJ-1271G. The associate editor coordinating the review of this paper and approving it for publication was Prof. Gianluca Lazzi.

A. Mahmood was with the Department of Electrical Engineering, University of Texas at Arlington, Arlington, TX 76013 USA. He is now with the Department of Electrical and Computer Engineering, Birck Nanotechnology Research Center, Purdue University, West Lafayette, IN 47907 USA (e-mail: amahmood@purdue.edu.; aamer Mahmood@ieee.org).

D. P. Butler and Z. Çelik-Butler are with the Department of Electrical Engineering, University of Texas at Arlington, Arlington, TX 76013 USA (e-mail: dbutler@uta.edu; zbutler@uta.edu; celikbutler@comcast.net; celikbutler@ieee.org).

Color versions of one or more of the figures in this paper are available online at <http://ieeexplore.ieee.org>.

Digital Object Identifier 10.1109/JSEN.2007.896560

an aerial platform like a conventional unmanned micro-aerial vehicle (UAV) that can be given sensory perception of temperature, pressure, air speed, humidity, etc., by pasting on a “smart skin”—a flexible substrate hosting sensors, electronics, and power sources like solar cells. This would be an improvement in the capabilities of an ordinary system yet a rigid conventional package would not be usable without major structural adjustments to the host platform. Another possible application is smart gloves for a surgeon performing remote surgery, thus allowing the surgeon to “feel.” The development of temperature sensors on flexible substrates is part of the strategic goal to develop “smart skin”—a flexible substrate hosting different type of sensors to monitor ambient temperature, pressure, humidity, air speed, acceleration, etc., along with the associated electronic circuitry and power sources like solar or fuel cells. This will make flexible systems-on-a-chip realizable. Such systems can be used in foldable electronics, form part of smart fabrics, lead to smart packaging for nonplanar commodities for applications in the fields of defense and surveillance, biomedicine, industrial monitoring, and testing, etc.

Most microelectromechanical systems (MEMS) devices require vacuum or hermetic packaging for optimum performance. Microbolometers are no exception and need vacuum encapsulation. The present work seeks to develop a vacuum package for bolometric thermal sensors on flexible substrates. Uncooled bolometric thermal detectors using the semiconducting phase of yttrium barium copper oxide (YBaCuO; commonly referred to as YBCO) have been successfully fabricated and tested [1]–[7]. The bolometric properties of this material have been well documented in literature. It is fully CMOS compatible and is a suitable candidate for future applications in large imaging arrays built atop a conventional CMOS read-out circuit. Bolometers using YBCO have also been successfully fabricated on flexible polyimide substrates [8]–[13]. These devices have performances comparable to the devices fabricated on rigid substrates. Bolometers being thermal detectors, perform best when they are thermally isolated from the ambient and preserve the heat produced in them due to incident infrared radiation. Thermal conduction is the major source of heat loss and as such a low thermal conductivity from the detector to the ambient/substrate is imperative for good performance. Micromachining the detector to isolate it from the ambient and using materials with low thermal conductance serves to this end. Operation in vacuum further reduces the thermal conductivity by eliminating enveloping air as a conduit of heat loss. Encapsulation using organic overcoats or sealing with an inorganic material have been the traditional ways to vacuum package [14]. Encapsulation is cheaper but has a limited lifespan primarily due to the permeation properties of

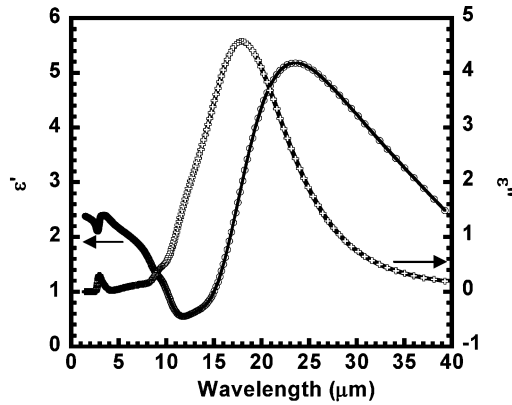


Fig. 1. Real ( $\epsilon'$ ) and imaginary ( $\epsilon''$ ) parts of the complex relative permittivity ( $\epsilon_r$ ) of ceramic  $\text{Al}_2\text{O}_3$  sputtered in a pure Ar environment at room temperature. Data was extracted using infrared variable angle spectroscopic ellipsometry.

the resin used. Inorganic seals are longer lasting but more expensive. Wafer and die level packaging [15], [16] are employed within this realm.

Vacuum packaging has traditionally been rigid, which defeats the purpose of detectors on flexible substrates. Device level packaging is an alternative that can provide a vacuum environment without sacrificing flexibility. It is also useful in an integrated multisensor system where some of the sensors might need vacuum packaging but others need to be exposed to the atmosphere.

## II. DESIGN OF A VACUUM CAVITY

In this work, a vacuum cavity is grown around the bolometer. This serves to provide a vacuum environment without sacrificing flexibility. Sacrificial polyimide layers are used to create the cavity and  $\text{Al}_2\text{O}_3$  has been used as the optical window material. Fuertes *et al.* [17] have reported high optical transmission in the near to far infrared region through  $\text{Al}_2\text{O}_3$  films deposited by spray pyrolysis. To determine the optical properties of the  $\text{Al}_2\text{O}_3$ , a sample was prepared by sputtering  $\text{Al}_2\text{O}_3$  on a Si wafer at room temperature in pure Ar environment at 10 mTorr. The complex relative permittivity ( $\epsilon(\lambda) = \epsilon'(\lambda) - j\epsilon''(\lambda)$ ) of  $\text{Al}_2\text{O}_3$  were extracted using infrared variable angle ellipsometry (Fig. 1). The imaginary component of the complex relative permittivity  $\epsilon''(\lambda)$  is a measure of the absorption of the electromagnetic energy in the material. It can be seen from Fig. 1 that sputtered  $\text{Al}_2\text{O}_3$  transmits infrared energy in the near and mid infrared region and starts absorbing from  $\sim 9 \mu\text{m}$  onwards with absorption peaking at  $\sim 18 \mu\text{m}$  before declining at longer wavelengths. The optical window in the vacuum cavity also serves as a pressure window with a pressure differential of  $\sim 1$  Atm across the surface. The suitability of  $\text{Al}_2\text{O}_3$  in the role of the pressure window was verified by testing its mechanical properties using CoventorWare based on the finite-element method (FEM). Moreover, the computer model of the vacuum cavity was subjected to physical bending by fixing one edge in space, while the opposite edge was moved towards the first edge—simulating the bending of the smart skin around a curved surface. The stresses produced in the  $\text{Al}_2\text{O}_3$  optical window up to  $180 \times 180 \mu\text{m}^2$  in lateral dimensions and  $3 \mu\text{m}$  thick were noted as a function of the radius of curvature (Fig. 2). It can be seen that the Mises

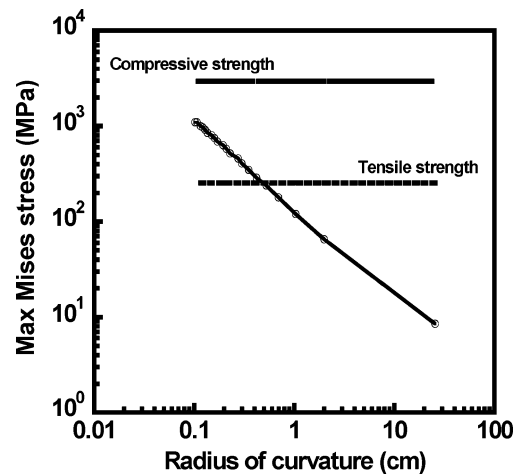


Fig. 2. Mises stresses produced in the  $\text{Al}_2\text{O}_3$  optical window of a vacuum cavity model versus the radius of curvature of the cavity. The data has been generated using FEM-based CoventorWARE. The tensile and compressive strengths of ceramic  $\text{Al}_2\text{O}_3$  [18] are also shown for reference.

stresses stayed less than 0.26 GPa—the tensile strength of ceramic  $\text{Al}_2\text{O}_3$  [18], up to a radius of  $\sim 1$  cm.

An equivalent thermal circuit of the bolometer and its package [19] was created to calculate the thermal conductance from the bolometer to the heat sink using the expression  $G_{\text{th}} = k(A/l)$ , where  $k$  is the material thermal conductivity,  $A$  is the cross-sectional area and  $l$  is the length of the heat channel. Given any particular material, the thermal conductance is a function of the physical dimensions of the heat channel which is a measure of the thermal isolation, i.e., the micromachining and the vacuum packaging. Different cases were studied ranging from the best case scenario; a model of a device isolated from the substrate with perfect micromachining and in a vacuum environment, to the worst case scenario: a device sitting atop residual partially micromachined sacrificial polyimide in the presence of air (to simulate a ruptured cavity). The best case thermal conductance (perfect micromachining) was calculated to be  $4.0 \times 10^{-6}$  W/K in vacuum. The thermal conductance was also calculated using numeric techniques. A model of the microbolometer was created using CoventorWARE. Material properties from [18] were used. The microbolometer was kept at a temperature of 301 K acting as the heat source, while the top of the  $\text{Al}_2\text{O}_3$  plugs as well as the edge of the support nitride layer (signifying the extent of the micromachined cavity) at 300 K acted as the heat sink. The thermal power  $P_{\text{th}}$  (W) flowing from the heat source to the heat sink due to this temperature differential  $\Delta T = 1$  K was calculated using FEM and was used to calculate the thermal conductance  $G_{\text{th}} = P_{\text{th}}/\Delta T$ . A value of  $5.1 \times 10^{-6}$  W/K was computed, which agrees well with the analytic calculation.

The same device in the presence of air (signifying a ruptured vacuum cavity) had a thermal conductance of  $1.4 \times 10^{-4}$  W/K. Such a discernable difference in  $G_{\text{th}}$  makes it a useful tool to gauge the quality of the vacuum cavity after fabrication. The calculated values of  $G_{\text{th}}$  were used as a benchmark for comparison to the measured  $G_{\text{th}}$  of the fabricated devices to evaluate the quality of the vacuum around the bolometer. The P15878G was removed from on top of  $\text{Al}_2\text{O}_3$  window layer.

### III. FABRICATION

Based on the computer designs, lithographical masks were prepared and devices were fabricated. The semiconducting phase of yttrium barium copper oxide (YBaCuO) was used as the bolometric material. Liquid polyimide PI 5878G was utilized to form the flexible substrate by spin casting onto the Si wafer with the spin speed and duration determining the final thickness after cure at  $\sim 275^\circ\text{C}$ . The glass transition temperature of the polyimide is about  $400^\circ\text{C}$ , which provides ample thermal budget downstream. It has excellent resistance to various reagents and etchants used in a typical CMOS fabrication process and is rated to have zero vapor pressure after curing, according to specifications. During fabrication, all material depositions except Al were done by rf sputtering in a pure Ar environment at 10 mTorr pressure. Al was deposited by thermal evaporation in a high vacuum environment.

Fabrication started with a  $3500\text{ \AA}$  layer of  $\text{Si}_3\text{N}_4$  on a Si wafer. This layer promotes adhesion to subsequent layers. This was followed by spin casting polyimide PI5878G on to a silicon wafer. The total thickness of  $24\text{ }\mu\text{m}$  was achieved by three depositions, each followed by a soft bake at  $110^\circ\text{C}$ – $115^\circ\text{C}$ . The polyimide coated wafer was then loaded into an oven at  $115^\circ\text{C}$  and the temperature gradually ramped up to  $275^\circ\text{C}$  to bake the polyimide for 4 h. A  $3500\text{ \AA}$  layer of  $\text{Si}_3\text{N}_4$  was deposited on the polyimide to promote adhesion between the polyimide and subsequent layers. The preceding two steps were skipped for the detectors on rigid Si substrate.  $4000\text{ \AA}$  of Al was then deposited to serve as the reflecting mirror. A  $2.5\text{-}\mu\text{m}$ -thick polyimide PI2610 was then spin-coated above the Al to serve as the sacrificial layer and cured as mentioned earlier. This was followed by  $3500\text{ \AA}$  of nitride to form the support membrane for the detector. Negative photoresist liftoff technique was used to pattern Ti arms and Au contacts. The Ti layer was  $1500\text{ \AA}$  thick and was covered with  $700\text{ \AA}$  of Au. Ti is used as the electrode arm since it is known to provide adequate electrical conduction while maintaining relatively low thermal conduction. Gold contacts provide an Ohmic contact between the Ti and the YBCO as well as forming the bond pads for subsequent characterization. After liftoff, the Au was patterned and etched off to leave only the contacts and the bond pads [Fig. 3(a1) and (a2)].  $3600\text{ \AA}$  of YBCO was then deposited, patterned and etched to form the bolometer pixel. Trenches were opened in the nitride layer to enable subsequent micromachining of the underlying sacrificial polyimide [Fig. 3(b1) and (b2)].

At this stage, the bolometer is complete and subsequent steps are used to build the vacuum cavity around it. Photodefinable polyimide PI2737 was spun on, patterned, and developed to form an approximately  $2\text{ }\mu\text{m}$  high sacrificial mesa on top of the detector [Fig. 3(c1) and (c2)].  $1.5\text{ }\mu\text{m}$  of  $\text{Al}_2\text{O}_3$  was then deposited to form the initial layer of the optical window above the mesa. Trenches were opened in the  $\text{Al}_2\text{O}_3$  layer [Fig. 3(d1) and (d2)] to micromachine the cavity underneath with oxygen plasma. The top polyimide PI2737 was etched first, in the process exposing the underlying PI2610 through the trenches in the support  $\text{Si}_3\text{N}_4$ . Both  $\text{Al}_2\text{O}_3$  and  $\text{Si}_3\text{N}_4$  layers are optically transparent and the progress in micromachining can be observed visually under a microscope. The extent of the lateral

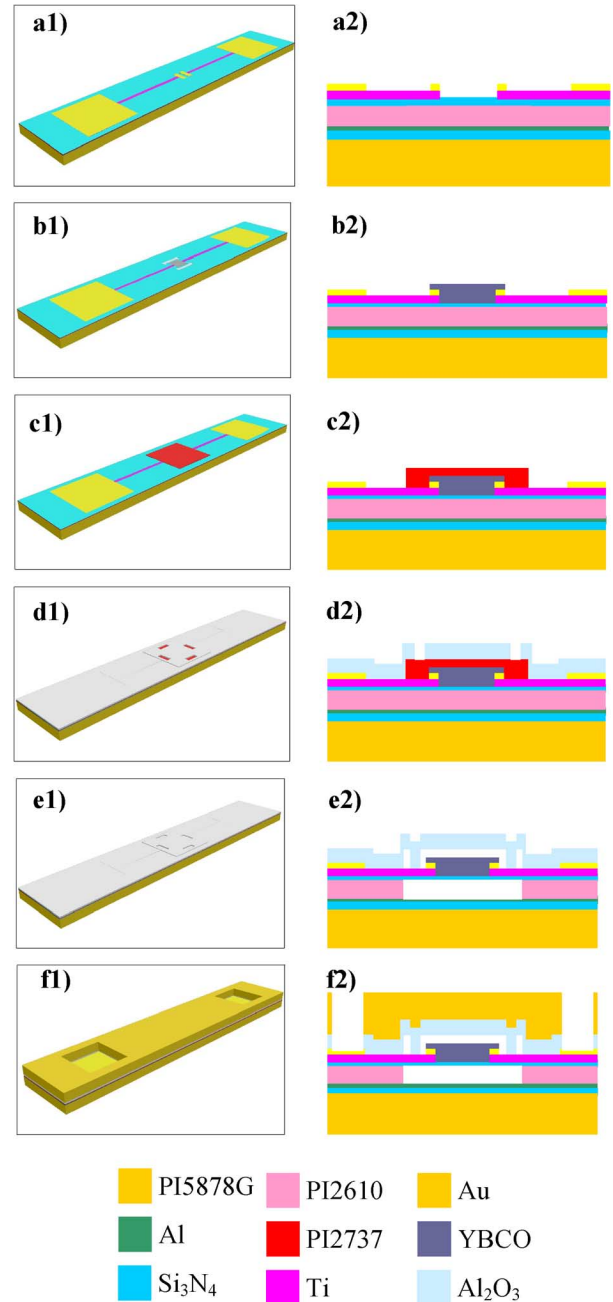


Fig. 3. Fabrication steps: a1) Model of Ti arms and Au bond pads and contacts. a2) Sectioned view through the center of model. b1) Model of YBCO pixel. b2) Sectioned view through the center of model. c1) Model of photodefinable PI2737 sacrificial mesa. c2) Sectioned view through the center of model. d1) Model of  $\text{Al}_2\text{O}_3$  with trenches above sacrificial mesa. d2) Sectioned view through the center of model. e1) Model of sealed vacuum cavity. e2) Sectioned view through the center of model. f1) Model of superstrate PI5878G. f2) Sectioned view through the center of model. (Dimensions not to scale.)

etch under the  $\text{Si}_3\text{N}_4$  support layer gives an idea of the etching under the bolometer pixel. The cavity can then be sealed shut by further deposition of  $\text{Al}_2\text{O}_3$  [Fig. 3(e1) and (e2)]. PI5878G was subsequently deposited on top of the device, exposed and developed above the bond pads. The  $\text{Al}_2\text{O}_3$  layer was etched above the bond pads to provide electrical access to the devices [Fig. 3(f1) and (f2)].

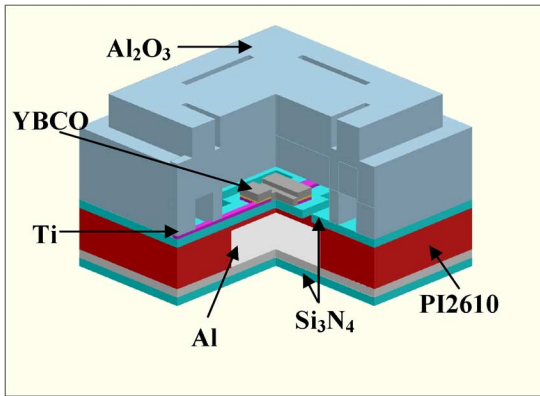


Fig. 4. Computer generated isometric view of sectioned vacuum cavity to show interior details. (Dimensions not to scale).

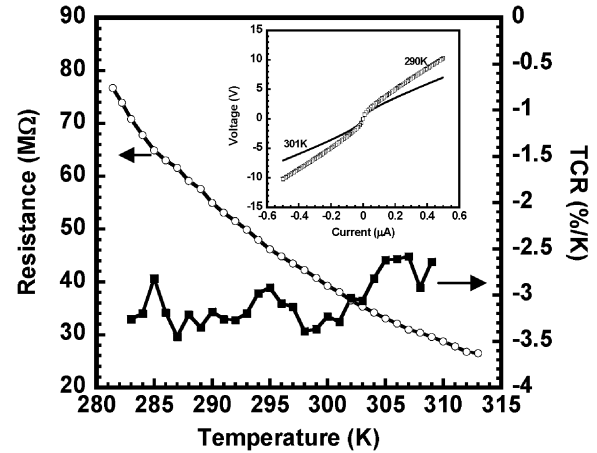


Fig. 6. Resistance and TCR versus temperature of DEV-R. (Inset) Nonlinear VI characteristics of the same device at 301 and 290 K.

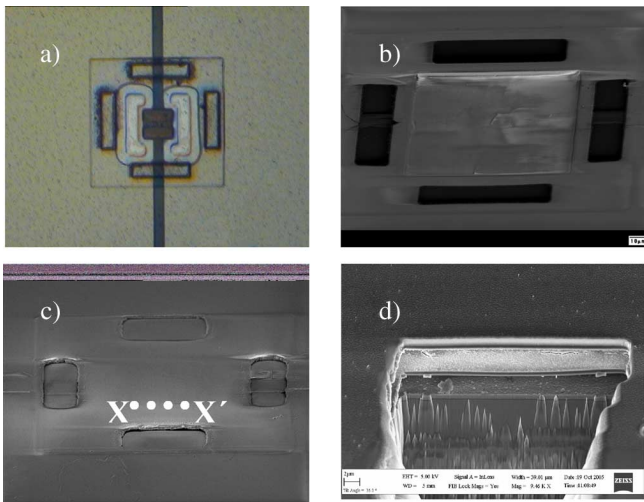


Fig. 5. a) Micromachined microbolometer under an optical microscope. b) SEM graph of unsealed microcavity showing  $\text{Al}_2\text{O}_3$  optical/pressure window and unsealed trenches. c) SEM graph of sealed microcavity showing  $\text{Al}_2\text{O}_3$  optical/pressure window and sealed trenches. d) Cross-sectional view of vacuum cavity at  $XX'$  in Fig. 5(c) showing  $\text{Si}_3\text{N}_4$  support membrane between micromachined spaces.

Fig. 4 shows a cut away model of the vacuum cavity containing a microbolometer on a supporting nitride membrane. Fig. 5(a) is an optical photo of a micromachined device. The extent of the micromachining can be seen through the transparent  $\text{Al}_2\text{O}_3$  and  $\text{Si}_3\text{N}_4$  layers. An SEM graph of a micromachined device prior to encapsulation is shown in Fig. 5(b). The completed sealed device is depicted in the SEM graph of Fig. 5(c). A cross-sectional cut is made at  $XX'$  with a focused ion beam to expose the nitride membrane between the micromachined cavities above and below [Fig. 5(d)].

The devices were diced, packaged and tested for electrical and optical properties.

#### IV. DETECTOR CHARACTERIZATION AND DISCUSSION

The characterization was done on devices without a PI5878 superstrate. The device resistance, in light of the device geometry ( $40 \times 40 \mu\text{m}^2$ ) and the materials used, was expected to be 150–200 k $\Omega$ , a fact corroborated by resistance measurements

using a probe station immediately after the detectors were fabricated. However, device resistance measured after completion was much higher than these values. It is suspected that the sacrificial polyimide PI2737 spun onto the YBCO detector attacks the pixel since it is in contact with it.

It was seen that after depositing the sacrificial polyimide, the detector resistance kept increasing until in some cases it was not possible to measure the resistance directly. The resistance of the device on flexible substrate (henceforth called DEV-F) was measured to be 86.7 M $\Omega$ , while that of the device on rigid substrate (henceforth called DEV-R) was 39.3 M $\Omega$ . The device resistance was measured also as a function of temperature. The temperature coefficient of resistance (TCR) of the bolometers was extracted using the relation [20], [21]

$$\text{TCR} = \alpha = 1/R(dR/dT) \quad (1)$$

where  $R$  is the bolometer resistance and  $T$  is the absolute temperature. DEV-F had a TCR of  $-3.7\% \text{ K}^{-1}$ , while the TCR for DEV-R was  $-3.4\% \text{ K}^{-1}$ , both at 300 K. These values are in agreement with the reported values of TCR for YBCO [6]–[10]. Fig. 6 shows the TCR and resistance of DEV-R as a function of temperature. The VI curves of the same device at two different temperatures are also shown.

The Arrhenius relation

$$R(T) = R_0 \exp(E_a/kT) \quad (2)$$

where  $k$  is Boltzmann's constant, was used to find  $R_0$  and the activation energy  $E_a$  from the resistance versus temperature data. DEV-F and DEV-R had  $R_0$  values of 902 and 2020  $\Omega$ , while  $E_a$  was calculated to be 0.30 and 0.26 eV, respectively. The thermal conductance of the device to the substrate was computed using the Joule heating method. A semiconductor parameter analyzer was used for this purpose to measure the device VI characteristics. In view of the high device resistance, the current sweep was kept between  $\pm 0.5 \mu\text{A}$  to minimize excessive heat dissipation in the bolometers. The nonlinear VI characteristics [Fig. 6 (inset)] show the effect of Joule heating. The VI data was used to plot the

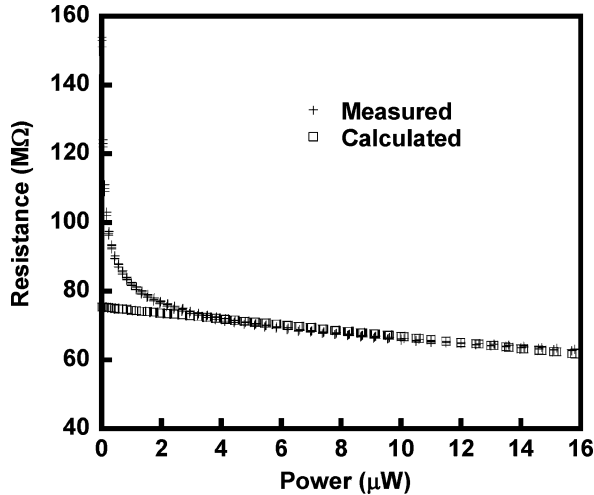


Fig. 7. Measured and calculated resistance of DEV-F versus dissipated power.

power dissipated in the device versus the resistance. Rice *et al.* [22] have shown that by using the relation

$$R(T) = R_{T_0} + \frac{1}{G_{th}} \frac{dR}{dT} P. \quad (3)$$

$G_{th}$  can be calculated from the slope of  $R$  versus  $P$  as in Fig. 7. Here,  $R(T)$  is the device resistance at temperature  $T$ ,  $R_{T_0}$  is the room temperature resistance, and  $P$  is the power dissipated in the detector calculated from the VI data.  $dR/dT$  was obtained from (1) and the measured TCR.

The room temperature  $G_{th}$  was  $3.7 \times 10^{-6}$  W/K for DEV-F. For DEV-R, the room temperature  $G_{th}$  was  $1.1 \times 10^{-6}$  W/K.

These thermal conductances were evaluated six months after the vacuum cavities had been fabricated. Fig. 7 shows the measured as well as calculated resistance for DEV-F as a function of dissipated power. The calculated resistance was found using (3).

The measured  $G_{th}$  is comparable, albeit lower than the expected values based on the analytic and FEM simulations for an intact cavity housing a fully micromachined microbolometer. This points to an intact microcavity, even six months after fabrication. The difference between the calculated and measured values is most likely due to a disparity in the modeled and fabricated geometries and needs to be explored further.

The optical characterization was done using a QTH lamp made by Oriol industries. A ZnSe lens was used to focus the infrared radiation onto the detector. To determine the power incident on the detector surface, an Oriol 70124 pyroelectric detector with a known responsivity of 1000 V/W was used for calibration purposes. This was then used to calculate the responsivity, detectivity, and noise equivalent power. Traditional bolometers need to be placed in a vacuum environment like a vacuum package with a ZnSe optical window for optimal performance. The device-level vacuum packaging, described here, allowed the measurements to be carried out in air. A mechanical chopper was used to modulate the optical signal. The devices were characterized with a fixed voltage bias. Voltage across a series resistance  $R_s$  ( $R_s < R_b$ ) was measured with a low noise amplifier and the output was fed to a dynamic signal analyzer. This way, current response of the bolometer  $R_b$  was evaluated.

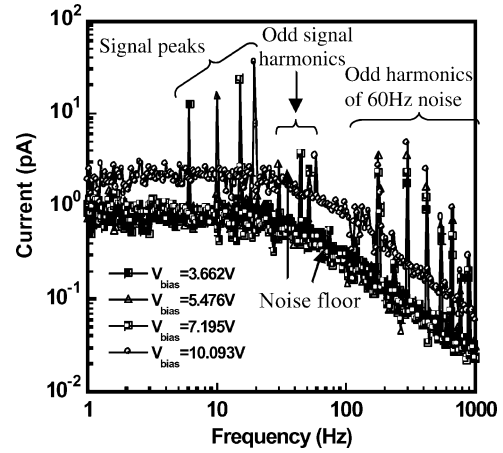


Fig. 8. Typical signal spectrum as a function of electrical frequency at different bias voltages. The signal peaks at different chopper frequencies as well as odd harmonics of the 60 Hz noise signal are clearly visible, while the 60 Hz noise peak has been suppressed for clarity.

Fig. 8 shows typical current spectra through the bolometer with different bias voltages across the detector for DEV-F. The signal peaks and odd harmonics as well as the odd harmonics of the 60 Hz noise peak are visible. The 60 Hz noise peak has been suppressed in this figure.

An important figure of merit is the detector responsivity: the detector output signal divided by the incident energy [20], [21]. The current responsivity  $\mathfrak{R}_I$ , is the output current through the bolometer due to incident infrared radiation energy modulated at angular frequency  $\omega$ .  $\mathfrak{R}_I$  is expressed as

$$\mathfrak{R}_I = \frac{-1}{(R_s + R_b)} \frac{\eta \alpha V_b}{G_{th} \left\{ 1 + \alpha \Delta T \left( \frac{R_b - R_s}{R_b + R_s} \right) \right\} \sqrt{1 + \omega^2 \tau_{eff}^2}}. \quad (4)$$

Here,  $\eta$  is the absorptivity of the infrared energy by the bolometer,  $V_b$  is the voltage across the bolometer, and  $\tau_{eff}$  is the effective thermal time constant of the detector, expressed as  $\tau_{eff} = C_{th}/G_{eff}$  in terms of the thermal capacitance and conductance. The effective thermal conductance can be expressed as

$$G_{eff} = G_{th} \left\{ 1 + \alpha \Delta T \left( \frac{R_b - R_s}{R_b + R_s} \right) \right\} \quad (5)$$

in terms of  $G_{th}$ , the physical thermal conductance between the bolometer and its surroundings, as defined earlier [21]. The cavity dimensions along the optical axis have to be designed carefully to achieve maximum power absorption on the detector plane. Slight variations in the dimensions like layer thicknesses or interlayer spacing can change the absorptivity significantly. At a modulation frequency of 5 Hz, DEV-F had a current responsivity of 61.3  $\mu A/W$  for  $V_b = 10.1$  V. At the same frequency, DEV-R exhibited a current responsivity of 50  $\mu A/W$  for  $V_b = 1.5$  V. The detectivity  $D^*$  of the devices was calculated by using the measured responsivity and noise. For a specific  $V_b$ , the detectivity can be evaluated as [20], [21]

$$D^* = \mathfrak{R}_I \frac{\sqrt{A \Delta f}}{\Delta I_n} \quad (6)$$

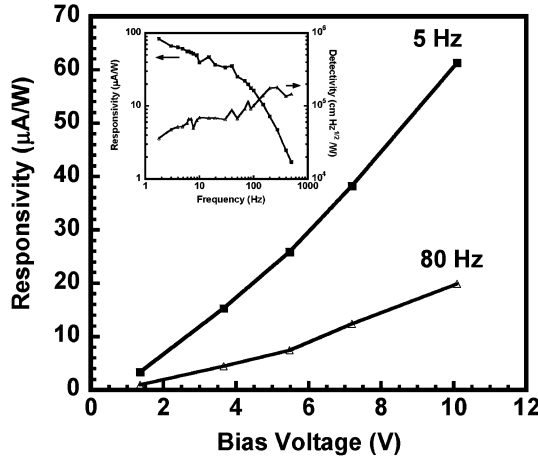


Fig. 9. Responsivity versus bias voltage of DEV-F in response to a broadband infrared radiation modulated at 5 and 80 Hz. (Inset) Current responsivity at a bias voltage of  $V_b = 10$  V and corresponding detectivity.

where  $A$  is the detector area and  $\Delta I_n$  is the noise signal over the electrical frequency bandwidth  $\Delta f$ . The noise includes the background noise, the temperature fluctuation noise, the Johnson noise, and the  $1/f$  noise in the YBCO bolometer.

DEV-F and DEV-R had maximum detectivities of  $3.1 \times 10^5$  cm-Hz<sup>1/2</sup>/W and  $1.1 \times 10^6$  cm-Hz<sup>1/2</sup>/W, respectively. Fig. 9 shows the responsivity and detectivity for DEV-F. Fig. 10 shows the responsivity and detectivity of DEV-R. The low detectivity is due to the relatively high noise exhibited by the devices. The sources of the noise need to be investigated and eliminated in future work.

Another important figure of merit is the noise equivalent power (NEP); the input power necessary to give a unity signal to noise ratio [20], [21]

$$\text{NEP} = \frac{\Delta I_n}{\mathfrak{R}_I}. \quad (7)$$

An NEP of  $7.7 \times 10^{-8}$  W/Hz<sup>1/2</sup> and  $2.7 \times 10^{-8}$  W/Hz<sup>1/2</sup> was measured at 5 Hz for DEV-F and DEV-R, respectively.

The thermal time constant of the devices with an applied bias, called the effective thermal time constant, was found from the measured responsivity data using the expression  $\tau_{\text{eff}} = 1/2\pi f_{-3 \text{ dB}}$ , where  $f_{-3 \text{ dB}}$  is the modulation frequency at which the detector has half the maximum responsivity [21]. Both DEV-F and DEV-R had  $f_{-3 \text{ dB}} \approx 50$  Hz corresponding to  $\tau_{\text{eff}} \approx 3.2$  ms. The corresponding thermal time constant can be calculated from the relation  $\tau_{\text{th}} = \tau_{\text{eff}} \{1 + \alpha \Delta T ((R_b - R_s)/(R_b + R_s))\}$  [21]. DEV-F had a thermal time constant  $\tau_{\text{th}} \approx 3.0$  ms, while DEV-R had a thermal time constant  $\tau_{\text{th}} \approx 3.3$  ms. The measured thermal capacitance  $C_{\text{th}}$  was extracted from the measured  $G_{\text{th}}$  and  $\tau_{\text{th}}$  using the relation  $C_{\text{th}} = \tau_{\text{th}} G_{\text{th}}$ . DEV-F and DEV-R had thermal capacitances of  $1.1 \times 10^{-8}$  J/K and  $3.3 \times 10^{-9}$  J/K, respectively. Using the volume and specific heat capacity of each material on the micromachined bridge, the theoretical thermal capacitance  $C_{\text{th}}$  of both the devices was computed to be  $2.0 \times 10^{-9}$  J/K, as the geometry is the same.

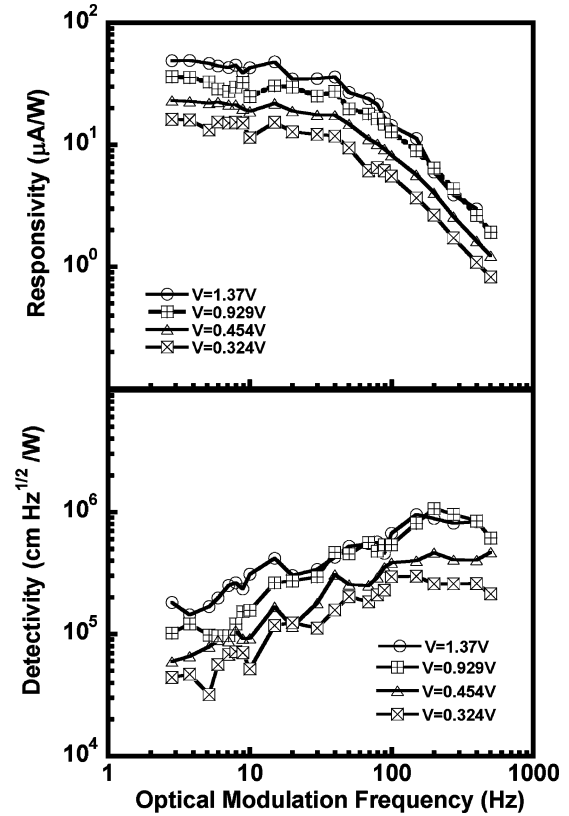


Fig. 10. Responsivity and detectivity versus optical modulation frequency of DEV-R.

For maximum responsivity, (4) reduces to

$$\mathfrak{R}_I^{\text{max}} = \frac{-\eta \alpha V_b}{G_{\text{eff}}(R_s + R_b)}. \quad (8)$$

Using the measured values of maximum responsivity  $\mathfrak{R}_I^{\text{max}}$ , TCR  $\alpha$ , effective thermal conductance  $G_{\text{eff}}$  and the known values of the voltage across the bolometer  $V_b$ , the series and bolometer resistances  $R_s$  and  $R_b$ , respectively, the absorptivity  $\eta$  has been calculated to be 4.7% and 7.7% for DEV-F and DEV-R, respectively.

## V. CONCLUSION

Device level vacuum packaged microbolometers have been designed, fabricated, and characterized. The vacuum cavity has been capped with an optical window of Al<sub>2</sub>O<sub>3</sub>, which also serves as a pressure window, since the cavity is in vacuum. The feasibility of the design was verified using FEM simulations. The thermal conductance of the device to the substrate was measured to be  $3.7 \times 10^{-6}$  W/K for a device on flexible PI5878G substrate and  $1.1 \times 10^{-6}$  W/K for a device on a rigid Si substrate. These values compare well to theoretical thermal conductivities calculated for these devices using analytical techniques, hence pointing to intact vacuum cavities. The flexible substrate bolometers exhibited a responsivity and detectivity of 61.3  $\mu\text{A/W}$  and  $5.2 \times 10^4$  cm-Hz<sup>1/2</sup>/W (at 5 Hz, and  $V_b = 10.1$  V), while the rigid substrate bolometers showed a responsivity and detectivity of 50.0  $\mu\text{A/W}$  and  $1.5 \times 10^5$  cm-Hz<sup>1/2</sup>/W (at 5 Hz, and  $V_b = 1.5$  V). An NEP of

TABLE I  
SUMMARY OF RESULTS

Name of device	DEV-F	DEV-R
Substrate	PI 5878G	Si
TCR (%/K) at 300K	-3.7	-3.4
$R_0$ ( $\Omega$ )	902	2020
$E_a$ (eV)	0.30	0.26
$G_{th}$ (measured) (W/K)	$3.7 \times 10^{-6}$	$1.1 \times 10^{-6}$
$R_b$ (M $\Omega$ )	86.7	39.3
$\Re_I$ @ 5 Hz ( $\mu$ A/W)	61.3 $V_b=10.1V$	50.0 $V_b=1.5V$
Maximum $\Re_I$ ( $\mu$ A/W)	83.2 @ 2Hz, $V_b=10.1V$	50.0 @ 5Hz, $V_b=1.5V$
$D^*$ @ 5 Hz (cm Hz <sup>1/2</sup> /W)	$5.2 \times 10^4$ $V_b=10.1V$	$1.5 \times 10^5$ $V_b=1.5V$
Maximum $D^*$ (cm Hz <sup>1/2</sup> /W)	$3.1 \times 10^5$ @ 398Hz, $V_b=7.2V$	$1.1 \times 10^6$ @ 200Hz, $V_b=0.9V$
NEP @ 5Hz (W/Hz <sup>1/2</sup> )	$7.7 \times 10^{-8}$	$2.7 \times 10^{-8}$
$C_{th}$ (measured) (J/K)	$1.1 \times 10^{-8}$	$3.3 \times 10^{-9}$
$\tau_{th}$ (ms)	3.0	3.3
$\eta$ (%)	4.7	7.7

$7.7 \times 10^{-8}$  W/Hz<sup>1/2</sup> and  $2.7 \times 10^{-8}$  W/Hz<sup>1/2</sup> was measured at 5 Hz for DEV-F and DEV-R, respectively.

Further work needs to be done to investigate a number of issues encountered during the development of these devices. Most importantly, the sacrificial PI2610 is believed to have attacked the YBCO detector, causing a manifold increase in the device resistance. Alternative sacrificial layers like photoresist may be tried to circumvent this problem. The cavity dimensions need to be investigated. This will enable the design of a tuned microcavity to improve power absorption in the microbolometer, and hence the bolometer performance. A detailed study also needs to be carried out to establish the device thermal conductance as a function of the micromachining/isolation to corroborate results obtained from FEM based modeling.

#### ACKNOWLEDGMENT

The authors wish to acknowledge the help of Y. Kenarangui who developed the Labview data acquisition routine used in the measurements presented in this paper. They also acknowledge

the help of Prof. D. Mueller at the University of North Texas and Dr. T. Tiwald at J. A. Woollam, Inc., for their help in measuring the permittivity of different materials used in this work.

#### REFERENCES

- [1] P. C. Shan, Z. Celik-Butler, D. P. Butler, and A. Jahanzeb, "Semiconducting YBaCuO thin films for uncooled infrared bolometers," *J. Appl. Phys.*, vol. 78, no. 12, pp. 7334–7339, 1995.
- [2] P. C. Shan, Z. Celik-Butler, D. P. Butler, A. Jahanzeb, C. M. Travers, W. Kula, and R. Sobolewski, "Investigation of semiconducting YBaCuO thin films: A new room temperature bolometer," *J. Appl. Phys.*, vol. 80, no. 12, pp. 7118–7123, 1996.
- [3] C. M. Travers, A. Jahanzeb, D. B. Butler, and Z. Celik-Butler, "Fabrication of semiconducting YBaCuO surface-micromachined bolometer arrays," *J. Microelectromech. Syst.*, vol. 6, no. 3, pp. 271–276, 1997.
- [4] A. Jahanzeb, C. M. Travers, Z. Celik-Butler, D. P. Butler, and S. G. Tan, "A semiconductor YBaCuO microbolometer for room temperature IR imaging," *IEEE Trans. Elect. Dev.*, vol. 44, no. 10, pp. 1795–1801, Oct. 1997.
- [5] J. E. Gray, Z. Celik-Butler, and D. P. Butler, "MgO sacrificial layer for micromachining uncooled Y-B-Cu-O IR microbolometers on Si<sub>3</sub>N<sub>4</sub> bridges," *IEEE J. Microelectromech. Syst.*, vol. 8, no. 2, pp. 192–199, 1999.
- [6] M. Almasri, D. P. Butler, and Z. Celik-Butler, "Self-supporting uncooled infrared microbolometers with low-thermal mass," *IEEE/ASME J. Microelectromech. Syst.*, vol. 10, no. 3, pp. 469–476, Sep. 2001.
- [7] M. Almasri, Z. Celik-Butler, D. P. Butler, A. Yaradanakul, and A. Yildiz, "Uncooled multimirror broad-band infrared microbolometers," *IEEE/ASME J. Microelectromech. Syst.*, vol. 11, no. 5, pp. 528–535, Oct. 2002.
- [8] S. A. Dayeh, D. P. Butler, and Z. Celik-Butler, "Micromachined infrared bolometers on flexible polyimide substrates," *Sens. Actuators A*, vol. 118, pp. 49–56, 2005.
- [9] A. Yaradanakul, D. P. Butler, and Z. Celik-Butler, "Uncooled infrared microbolometers on a flexible substrate," *IEEE Trans. Electron Devices*, vol. 49, pp. 930–933, May 2002.
- [10] A. Mahmood, S. A. Dayeh, D. P. Butler, and Z. Celik-Butler, "Micro-machined infrared sensor arrays on flexible polyimide substrates," in *Proc. IEEE Sensors Conf.*, Oct. 2003, vol. 2, pp. 777–782.
- [11] A. Yildiz, Z. Celik-Butler, and D. P. Butler, "Microbolometers on a flexible substrate for infrared detection," *IEEE Sensors J.*, vol. 4, no. 1, pp. 112–117, Feb. 2004.
- [12] A. Mahmood, A. Dave, Z. Celik-Butler, and D. Butler, "Wafer level self packaged infrared microsensors," in *Proc. SPIE*, 2004, vol. 3666, pp. 415–420.
- [13] A. Mahmood, D. P. Butler, and Z. Celik-Butler, "Micromachined bolometers on polyimide," *Sens. Actuators A*, accepted for publication.
- [14] R. R. Tummala, *Fundamentals of Microsystems Packaging*. New York: McGraw-Hill, 2001, pp. 580–609.
- [15] B. Lee, S. Seok, and K. Chun, "A study on wafer level vacuum packaging for MEMS devices," *J. Micromech. Microeng.*, vol. 13, pp. 663–669, 2003.
- [16] Y.-T. Cheng, H. Wan-Tai, K. Najafi, C. T.-C. Nguyen, and L. Lin, "Vacuum packaging technology using localized aluminum/silicon-to-glass bonding," *IEEE/ASME J. Microelectromech. Syst.*, vol. 11, no. 5, pp. 556–565, Oct. 2002.
- [17] M. Aguilar-Frutis, M. Garcia, C. Falcony, G. Plesch, and S. Jimenez-Sandoval, "A study of the dielectric characteristics of aluminum oxide thin films deposited by spray pyrolysis from Al(acac)<sub>3</sub>," *Thin Solid Films*, vol. 389, no. 1–2, pp. 200–206, 2001.
- [18] J. F. Shackelford and W. Alexander, Eds., *CRC Materials Science and Engineering Handbook*, 3rd ed. Boca Raton, FL: CRC, 2001.
- [19] R. R. Tummala, *Fundamentals of Microsystems Packaging*. New York: McGraw-Hill, 2001, pp. 212–263.
- [20] E. L. Dereniak and G. D. Boreman, *Infrared Detectors and Systems*. New York: Wiley, 1996, pp. 407–413.
- [21] R. A. Wood, "Monolithic silicon microbolometer arrays," in *Semiconductors and Semimetals Vol. 47: Uncooled Infrared Imaging Arrays and Systems*, P. W. Kruse and D. D. Skatrud, Eds. New York: Academic, 1997.
- [22] J. P. Rice, E. N. Grossman, L. J. Borchardt, and D. A. Rudman, "Higher Tc superconducting antenna-coupled microbolometer on silicon," in *Proc. SPIE*, 1994, vol. 2159, pp. 98–109.

**Aamer Mahmood** (S'99) was born in Pakistan in 1970. He received the B.E. degree in electrical engineering from N-W.F.P. University of Engineering and Technology, Peshawar, Pakistan, in 1992, the M.S. degree in electrical engineering from the University of Engineering and Technology, Lahore, Pakistan, in 1999, and the Ph.D. degree in electrical engineering from the University of Texas at Arlington in August 2006, where he worked on sensors on flexible substrates, device level vacuum packaging and MEMS based tunable infrared resonators.

He is currently engaged in Postdoctoral Research in the the Department Electrical and Computer Engineering, Purdue University, West Lafayette, IN. He has worked in industry in Pakistan and his graduate and professional experience spans the areas of electromagnetic scattering, MEMS sensors, and opto-electromechanical systems development.

**Donald P. Butler** (S'84–M'87–SM'98) received the B.A.Sc. degree in engineering science: physics option from the University of Toronto, Toronto, ON, Canada, in 1980, and the M.S. and Ph.D. degrees in electrical engineering from the University of Rochester, Rochester, NY, in 1981 and 1986, respectively.

He performed his graduate research at the Laboratory for Laser Energetics investigating the nonequilibrium behavior of superconductor thin films in response to picosecond electrical and optical excitations. He continued his graduate research as a Research Associate in 1986. In 1987, he joined the Department of Electrical Engineering, Southern Methodist University, as an Assistant Professor. In 1993, he was promoted to the rank of Associate Professor and Professor in 2001. He joined the Faculty of Electrical Engineering at the University of Texas at Arlington in 2002. He has published more than 100 journal articles and conference presentations and holds four patents. His current research is focused on microsensors, uncooled infrared detection, and other microelectromechanical devices (MEMS).

Dr. Butler is a recipient of the IEEE Third Millennium Medal. He is a member of the Optical Society of America. He is a Topical Editor for *Applied Optics*. His service includes being the Chair for the 2001 IEEE Emerging Technologies Symposium on Broadband Communications for the Internet Era and serving on the Steering Committee for the 2004 International Microwave Symposium.

**Zeynep Çelik-Butler** (S'84–M'87–SM'98) received received dual B.S. degrees in electrical engineering and physics from Bogaziçi University, Istanbul, Turkey, in 1982, and the M.S. and Ph.D. degrees in electrical engineering from the University of Rochester, Rochester, NY, in 1984 and 1987, respectively.

She is a Professor of Electrical Engineering and Director of Nanotechnology Research and Teaching Facility, University of Texas at Arlington. She was an IBM Predoctoral Fellow from 1983 to 1984, and an Eastman Kodak Predoctoral Fellow from 1985 to 1987. She joined the Department of Electrical Engineering, Southern Methodist University (SMU) in 1987 as an Assistant Professor; was tenured and promoted to Associate Professor in 1993. She was the holder of the J. Lindsay Embrey Trustee Assistant Professorship from 1990 to 1993. She served as the Assistant Dean of Graduate Studies and Research at SMU from 1996 to 1999 and was a Professor of Electrical Engineering from 1999 to 2002. She has four patents, four book chapters, and over 140 journal and conference publications in these fields. Her research interests include noise in electronic and photonic devices, microelectromechanical systems, and infrared and pressure sensors.

Dr. Çelik-Butler is a member of Eta Kappa Nu, and the American Physical Society. She is a Distinguished Lecturer for the IEEE-Electron Devices Society. She has received several awards including the IEEE-Dallas Section Electron Devices Society Outstanding Service Awards (1995, 1997), the IEEE—Electron Devices Society, Service Recognition Award (1995, 2003), the Outstanding Electrical Engineering Graduate Faculty Awards (1996, 1997, 2001), SMU Sigma Xi Research Award (1997), and the UTA Outstanding Research Achievement Award (2006). She served in various technical committees including 1988, 1989 IEEE-IEDM's and Annual Symposia on Electronic Materials, Processing and Characterization (1989–1992), and International Conference on Noise in Physical Systems and 1/f Fluctuations (ICNF) (1993, 1999, 2001). She was the General Chair of TEXMEMS II Workshop. She was one of the founding editors of *Fluctuation and Noise Letters* and served in this capacity until 2005. Currently, she serves on the Executive Committee for TEXMEMS workshops and is a member of the International Advisory Committee for ICNF.